

# Interaction of molybdenum hexacarbonyl with dehydroxylated alumina thin films at high temperatures: Formation and removal of surface carbides

Y. Wang, F. Gao, W.T. Tysoe\*

*Department of Chemistry and Biochemistry, Laboratory for Surface Studies, University of Wisconsin-Milwaukee, Milwaukee, WI 53211, USA*

Received 1 March 2005; received in revised form 25 March 2005; accepted 28 March 2005

Available online 11 May 2005

## Abstract

The reaction of  $\text{Mo}(\text{CO})_6$  with thin films of dehydroxylated alumina grown on a  $\text{Mo}(1\ 0\ 0)$  substrate above 500 K is studied in ultrahigh vacuum using temperature-programmed desorption and Auger and X-ray photoelectron spectroscopies. This results in the formation of a molybdenum carbide that incorporates a small amount of oxygen, where MoC is formed initially, becoming closer to  $\text{Mo}_2\text{C}$  as the  $\text{Mo}(\text{CO})_6$  exposure increases. Heating the (oxy)carbide-covered surface desorbs CO in two states at  $\sim 1130$  and 1320 K. Forming the alumina films with  $\text{H}_2^{18}\text{O}$  shows that the majority of the oxygen in the CO derives from the substrate. The lower-temperature desorption state arises from both oxycarbide decomposition and alumina reduction by the carbide, while the high-temperature state results only from reduction of the alumina, finally resulting in the formation of a MoAl alloy.

© 2005 Elsevier B.V. All rights reserved.

**Keywords:** X-ray photoelectron spectroscopy; Temperature-programmed desorption; Auger spectroscopy; Chemisorption; Molybdenum hexacarbonyl; Dehydroxylated alumina thin films

## 1. Introduction

Molybdenum hexacarbonyl derived catalysts are active for a number of reactions including olefin hydrogenation and metathesis [1–12]. The realistic catalysts system is mimicked in the following by decomposing  $\text{Mo}(\text{CO})_6$  on a thin film of dehydroxylated alumina grown on a  $\text{Mo}(1\ 0\ 0)$  substrate. This approach has several advantages. First, it allows model systems to be prepared that resemble the high-surface area catalysts. Second, the alumina film is sufficiently thin that charging problems can be avoided so that it allows conventional electron- and photon-based spectroscopies to be exploited. The interaction between molybdenum hexacarbonyl and alumina thin films at low temperatures has been studied in ultrahigh vacuum (UHV) by us [13–16] and others [17].  $\text{Mo}(\text{CO})_6$  desorbs intact below  $\sim 250$  K and also decomposes to form strongly bound species, which decompose to desorb CO [13,15] and has been identified on aluminas with various

degrees of hydroxylation as an oxalate species [13,15,16]. Unfortunately, only relatively small molybdenum coverages (a few percent of a monolayer) can be achieved in ultrahigh vacuum. Larger coverages can be obtained by illuminating adsorbed  $\text{Mo}(\text{CO})_6$  with ultraviolet radiation [18–20] or electrons [16]. The interaction of  $\text{Mo}(\text{CO})_6$  with metallic aluminum at high temperatures has been investigated recently [21]. It was found that a surface carbide/oxycarbide film is formed following molybdenum carbonyl reaction with the surface at 700 K. Heating this surface to above  $\sim 1200$  K desorbs CO and forms a MoAl alloy. This paper presents results on the decomposition of  $\text{Mo}(\text{CO})_6$  at high temperatures on a thin dehydroxylated alumina (DA) film grown on  $\text{Mo}(1\ 0\ 0)$ .

## 2. Experimental

Temperature-programmed desorption (TPD) data and X-ray photoelectron and Auger spectra were collected in ultrahigh vacuum chambers operating at base pressures of  $< 2 \times 10^{-10}$  Torr that have been described in detail elsewhere

\* Corresponding author. Tel.: +1 414 229 5222; fax: +1 414 229 5036.  
E-mail address: [wtt@uwm.edu](mailto:wtt@uwm.edu) (W.T. Tysoe).

[21,22]. Briefly, TPD data were collected using a Dycor quadrupole mass spectrometer placed in line of sight of the sample. Auger spectra were collected using an electron beam energy of 3 keV and the first-derivative spectrum obtained by numerical differentiation [22]. XPS data were collected using a Specs X-ray source and double-pass, cylindrical mirror analyzer with an Mg K $\alpha$  X-ray power of 250 W and a pass energy of 50 eV [21].

The Mo(1 0 0) substrate was cleaned using a standard procedure, which consisted of argon ion bombardment (2 kV, 1  $\mu$ A/cm<sup>2</sup>) and any residual contaminants were removed by briefly heating to 2000 K in vacuo. The resulting Auger spectrum showed no contaminants. A dehydroxylated alumina thin film was formed by evaporating aluminum onto Mo(1 0 0) [23]. The aluminum was oxidized at  $\sim$ 650 K by water vapor from a capillary doser at a background chamber pressure of  $\sim$ 1  $\times$  10<sup>-8</sup> Torr, leading to a pressure at the sample of  $\sim$ 2  $\times$  10<sup>-6</sup> Torr using an enhancement factor of 200 determined previously [22]. Following water oxidation, the sample was annealed gradually to  $\sim$ 1300 K for several minutes to remove surface hydroxy groups. TPD shows no water desorption following this treatment. This process was repeated until the alumina film was sufficiently thick that no substrate molybdenum signals were detected using Auger or XPS. Note that full oxidation of aluminum is generally difficult in UHV [24] but can be achieved using this approach when only a very thin aluminum film is deposited during each deposition-oxidation cycle.

Molybdenum hexacarbonyl (Aldrich, 99%) was transferred to a glass vial, connected to the gas-handling line of the chamber and purified by repeated freeze-pump-thaw cycles, followed by distillation, and its purity was monitored using mass and infrared spectroscopies. This was also dosed onto the surface via a capillary doser to minimize background contamination. The exposures in Langmuir (1 L = 1  $\times$  10<sup>-6</sup> Torr s) are corrected using the same enhancement factor of 200 [22].

### 3. Results

Fig. 1(a) shows the Auger spectra of Mo(CO)<sub>6</sub> adsorbed on dehydroxylated alumina at 700 K as a function of exposure, where the exposures are indicated adjacent to the corresponding spectrum. This reveals that the peak-to-peak intensities of the molybdenum (119, 160, 186 and 221 eV kinetic energy) and carbon KLL transitions (271 eV kinetic energy) increase with Mo(CO)<sub>6</sub> exposure, while the aluminum (53 eV kinetic energy, Al<sup>3+</sup>) and oxygen ( $\sim$ 510 eV kinetic energy) features decrease. Note that the clear break on the high-energy side of the 53 eV Auger peak (marked with an arrow) suggests complete oxidation of aluminum [24]. The typical shape of the carbon KLL Auger feature indicates the presence of carbide.

Fig. 1(b) displays expanded regions for the molybdenum Auger transitions. An Auger spectrum of the clean Mo(1 0 0) substrate is also shown. The kinetic energies of adsorbed

molybdenum are close to those of Mo(1 0 0), suggesting that the deposited molybdenum is metallic or has a low oxidation state.

Fig. 1(c) shows the results of annealing the sample to higher temperatures. Between 1000 and 1200 K, the carbon signal intensity increases to some extent, suggesting carbon diffusion to the surface during annealing. More pronounced changes occur at 1300 K where, in addition to a decrease in carbon signal intensity, an aluminum feature appears at 65.7 eV due to Al<sup>0</sup> formation [25], which persists up to a temperature of 1500 K.

Mo(CO)<sub>6</sub> was also adsorbed on dehydroxylated alumina at 500 and 600 K (data not shown) and yielded identical behavior as shown in Fig. 1(a). The resulting Mo<sub>186 eV</sub>/Al<sub>53 eV</sub> and C<sub>271 eV</sub>/Mo<sub>186 eV</sub> peak-to-peak ratios are plotted in Fig. 2(a) and (b), respectively. The data of Fig. 2(a) reveals a relatively constant uptake of molybdenum on the surface with reactive sticking probability increasing with sample temperature.

The C<sub>271 eV</sub>/Mo<sub>186 eV</sub> Auger peak-to-peak intensity ratio is converted to a C/Mo stoichiometry (plotted on the right coordinate of Fig. 2(b)) using the Auger sensitivity factors for molybdenum (1.278) and carbon (0.614) [26]. At low Mo(CO)<sub>6</sub> exposures, the Mo:C ratio is approximately unity indicating the initial formation of MoC. The ratio decreases rapidly up to an exposure of  $\sim$ 200 L and more slowly thereafter. This suggests that the carbide formed at higher Mo(CO)<sub>6</sub> exposures becomes closer to Mo<sub>2</sub>C and a similar behavior was found when reacting Mo(CO)<sub>6</sub> with metallic aluminum [21]. It has been demonstrated that the deposited film contains a tiny amount of oxygen when reacting Mo(CO)<sub>6</sub> with metallic aluminum [21]. However, it has been found previously that, during the initial stages of Mo oxidation (before stoichiometric oxides are formed), the positions of the molybdenum Auger transitions do not vary significantly [27]. It has been suggested [28], however, that the peak-to-peak intensity ratios of the molybdenum Auger transitions are more sensitive to molybdenum oxidation state. For pure Mo(1 0 0), the ratio  $I_{119 eV}/I_{186 eV} = 0.19$ ,  $I_{160 eV}/I_{186 eV} = 0.37$ , and  $I_{221 eV}/I_{186 eV} = 0.88$ . If molybdenum is oxidized, the ratios  $I_{119 eV}/I_{186 eV}$  and  $I_{160 eV}/I_{186 eV}$  are expected to increase and the ratio  $I_{221 eV}/I_{186 eV}$  to decrease. In order to establish whether the films grown on DA are slightly oxidized, these ratios are plotted versus Mo(CO)<sub>6</sub> exposure at 500 (Fig. 3(a)), 600 K (Fig. 3(b)) and 700 K (Fig. 3(c)), and as a function of annealing temperature (Fig. 3(d)). The results suggest molybdenum is slightly oxidized at all deposition temperatures (Fig. 3(a–c)). It should be mentioned that, for low Mo(CO)<sub>6</sub> exposures at 500 K, the deposited Mo is less oxidized than that grown at higher temperatures. The data in Fig. 3(d) show that molybdenum reduces at higher temperatures and, at 1500 K, is present as Mo(0).

The corresponding XPS narrow scans are displayed in Fig. 4. Fig. 4(a) shows the Al 2p region as a function of Mo(CO)<sub>6</sub> exposure yielding an Al 2p binding energy of

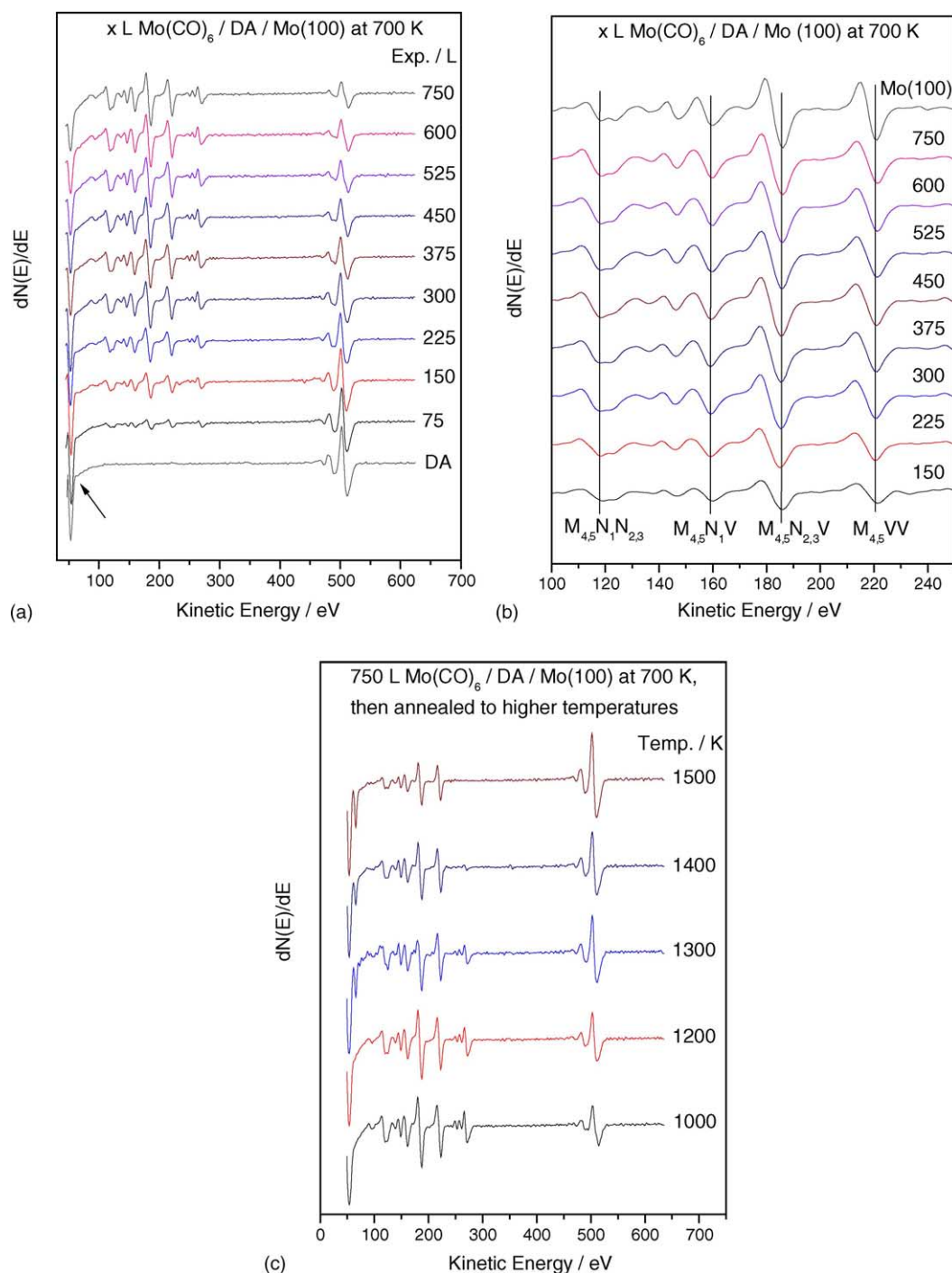


Fig. 1. Auger spectra of (a) Mo(CO)<sub>6</sub> adsorbed on dehydroxylated alumina as a function of exposure, where exposures are marked adjacent to the corresponding spectrum, (b) an enlarged depiction of (a), emphasizing the Mo transitions, and (c) the effect of heating a surface exposed to 750 L of Mo(CO)<sub>6</sub> at 700 K to various temperatures, where annealing temperatures are marked adjacent to the corresponding spectrum.

74.6 eV, in good agreement with the Al 2p BE of stoichiometric  $\gamma$ -Al<sub>2</sub>O<sub>3</sub> [29]. The Al 2p signal intensity decreases with increasing Mo(CO)<sub>6</sub> exposure, due to attenuation of the emitted photoelectrons by the growing film. The C 1s region in Fig. 4(b) reveals that a small amount of carbon is deposited on the surface. This has a BE of  $\sim$ 282.5 eV, corresponding to carbide in accord with the Auger lineshape (Fig. 1). Oxi-

dation of the carbide would yield a shoulder at 283.5–284 eV [30], but the weak C 1s signal precludes any conclusions being reached on whether an oxycarbide is formed. The Mo 3d region (Fig. 4(c)) displays Mo 3d<sub>5/2</sub> features at 228.1 and 229 eV BE, higher than the metallic Mo substrate feature at 227.4 eV. Fig. 4(d) shows the corresponding O 1s region, where the intensity decreases with increasing Mo(CO)<sub>6</sub> expo-

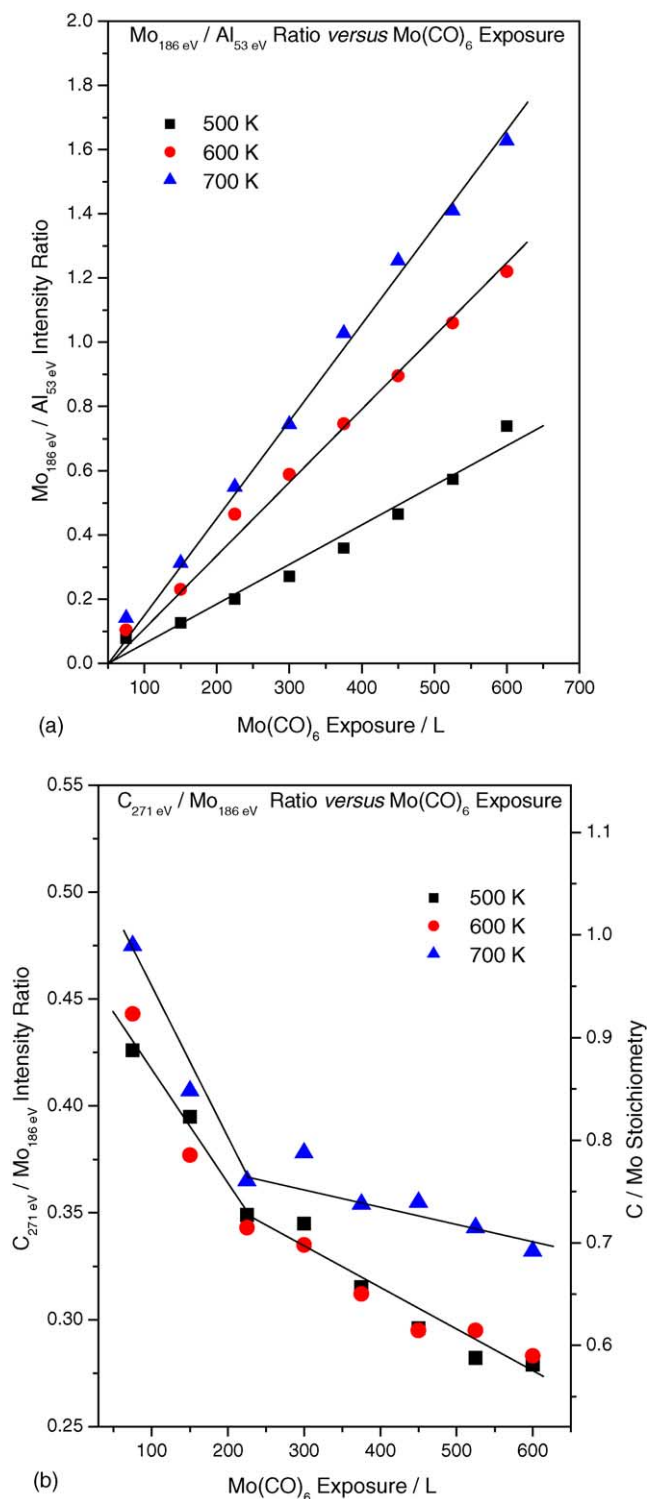


Fig. 2. (a) Plot of the Mo<sub>186 eV</sub>/Al<sub>54 eV</sub> peak-to-peak Auger intensity ratio and (b) the C<sub>271 eV</sub>/Mo<sub>186 eV</sub> peak-to-peak Auger ratio for Mo(CO)<sub>6</sub> adsorbed on dehydroxylated alumina at 500 K (■), 600 K (●) and 700 K (▲).

sure in the same fashion as the Al 2p features (Fig. 4(a)) also due to attenuation of the substrate signal due to the presence of the film. The O 1s binding energy is 531.6 eV, corresponding to aluminum oxide [29].

Narrow scan XP spectra are displayed in Fig. 5 following 700 L Mo(CO)<sub>6</sub> exposure to dehydroxylated alumina at 700 K as a function of annealing temperature. Fig. 5(a) displays the Al 2p region, where a slight shift in peak position from 74.8 to 75.0 eV is found as the sample is annealed from 700 to 1200 K. A larger shift occurs above 1300 K, from 75.0 to 75.8 eV. This chemical shift is accompanied by removal of carbon from the surface (Fig. 5(b)). The Mo 3d region (Fig. 5(c)) shows that, during annealing from 700 to 1200 K, the Mo 3d<sub>5/2</sub> features shifts from 228.1 to 227.4 eV, while on heating to above 1300 K, the intensity of the Mo 3d signal increases and the binding energy decreases to 272.1 eV (0.3 eV below that of metallic molybdenum). Fig. 5(d) displays the O 1s region where the O 1s feature remains reasonably constant at 531.6 eV BE up to ~1200 K and shifts to ~533 eV on heating to above 1200 K. This shift accompanies that observed in the Al 2p spectra (Fig. 5(a)) and will be discussed in more detail below.

The data of Fig. 4(c) show that only a limited amount of molybdenum is deposited on the DA surface following a Mo(CO)<sub>6</sub> exposure of 700 L at 700 K. In order to investigate the behavior of larger molybdenum coverages, DA was exposed to 5000 L of Mo(CO)<sub>6</sub> at 700 K and subsequently annealed to higher temperatures. The resulting XPS survey spectrum is plotted in Fig. 6(a). The spectra of DA, and the surface following a 700 L Mo(CO)<sub>6</sub> exposure are also plotted for direct comparison. This confirms that the 5000 L Mo(CO)<sub>6</sub> exposure results in larger molybdenum coverages and the Mo 3d region is shown, as a function of annealing temperature, in Fig. 6(b). This reveals that the Mo 3d<sub>5/2</sub> binding energy is 227.4 eV (identical to that of clean Mo(100)) at 700 K, which decreases gradually during annealing so that, at 1300 K and above, it is 227.1 eV. The corresponding Al 2p, C 1s and O 1s regions are not plotted since these show similar behavior as in Fig. 5.

The 28 amu (CO) TPD spectra collected at a heating rate of 15 K/s are displayed in Fig. 7(a) following Mo(CO)<sub>6</sub> exposures of 75 and 150 L on dehydroxylated alumina at 700 K. Two CO desorption states are observed; a broad desorption state at ~1120 K and a sharper one at ~1320 K. After initially dosing a dehydroxylated alumina surface with 75 L of Mo(CO)<sub>6</sub> and collecting a TPD spectrum (so after heating to ~1440 K), the sample was again exposed to 75 L of Mo(CO)<sub>6</sub> at 700 K, without cleaning the sample, and another TPD spectrum collected. The resulting data are displayed in Fig. 7(b), where the label adjacent to the spectrum indicates the number of times the procedure was repeated so that “1” indicates adsorption on clean dehydroxylated alumina and reproduces the spectrum shown in Fig. 7(a). Drastic changes are observed for each spectrum, so that, following the second Mo(CO)<sub>6</sub> dose, the 1120 K state is much more intense, the 1320 K desorption state is absent, and an additional intense state appears at ~1030 K. Following the third and fourth carbonyl doses, these desorption states intensify and the 1030 K state shifts slightly to lower temperatures.

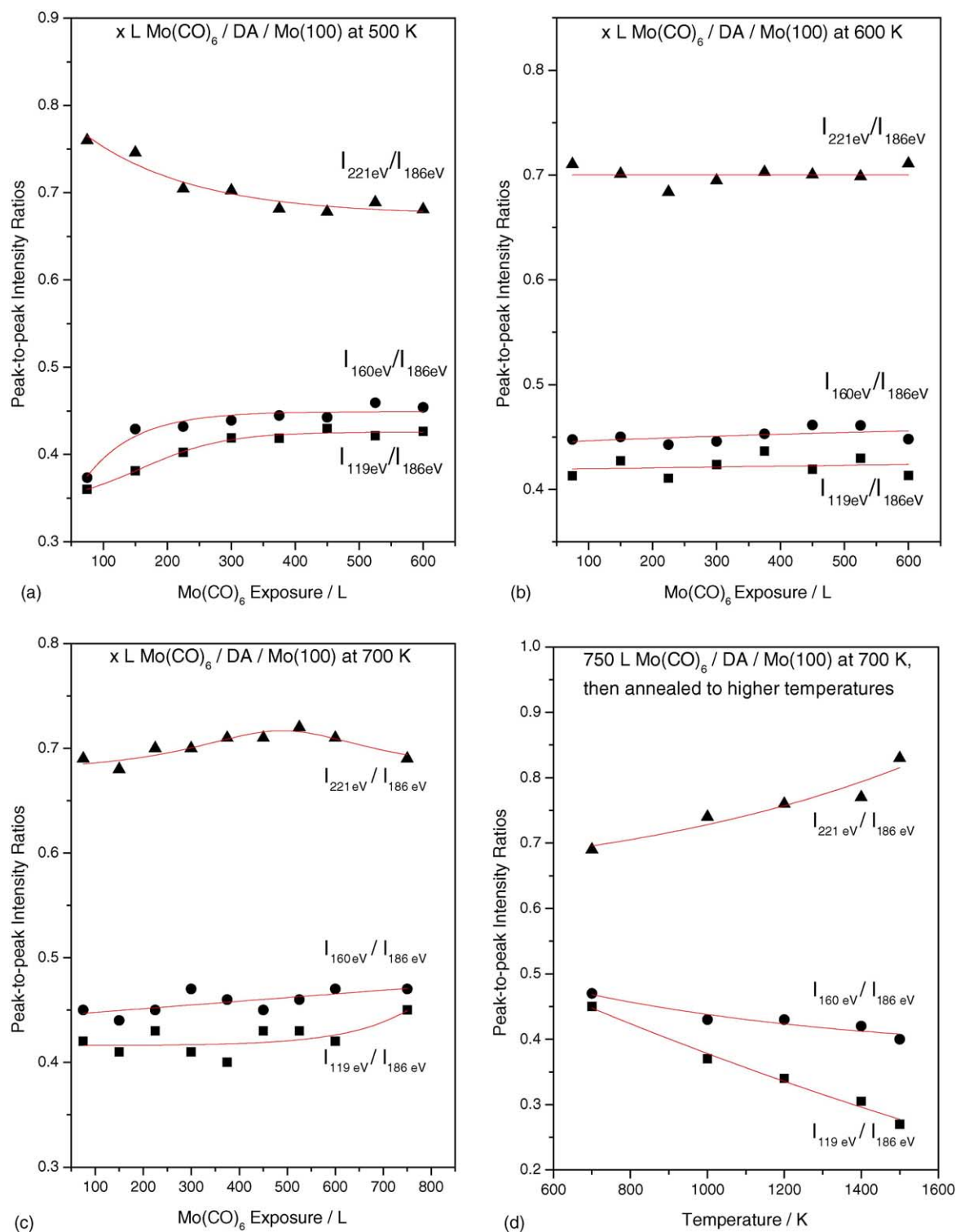


Fig. 3. Plot of the Auger peak-to-peak intensity ratios  $I_{221\text{eV}}/I_{186\text{eV}}$  (▲),  $I_{160\text{eV}}/I_{186\text{eV}}$  (●) and  $I_{119\text{eV}}/I_{186\text{eV}}$  (■) for the deposition of Mo(CO)<sub>6</sub> on dehydroxylated alumina at (a) 500 K, (b) 600 K and (c) 700 K as a function of Mo(CO)<sub>6</sub> exposure. Figure (d) shows the evolution of these intensity ratios as a function of annealing temperature.

Fig. 7(c) displays the corresponding Auger spectra of the surfaces before (1, 2, 3 and 4) and after (1a, 2a, 3a and 4a) each experiment shown in Fig. 7(b). Following Mo(CO)<sub>6</sub> adsorption on clean, dehydroxylated alumina

and heating to ~1300 K, an aluminum LVV Auger feature appears at 65.7 eV kinetic energy (Fig. 7(c), Spectrum 1a) indicative of the presence of metallic aluminum. Exposure of this surface to 75 L of Mo(CO)<sub>6</sub> (Fig. 7(c),

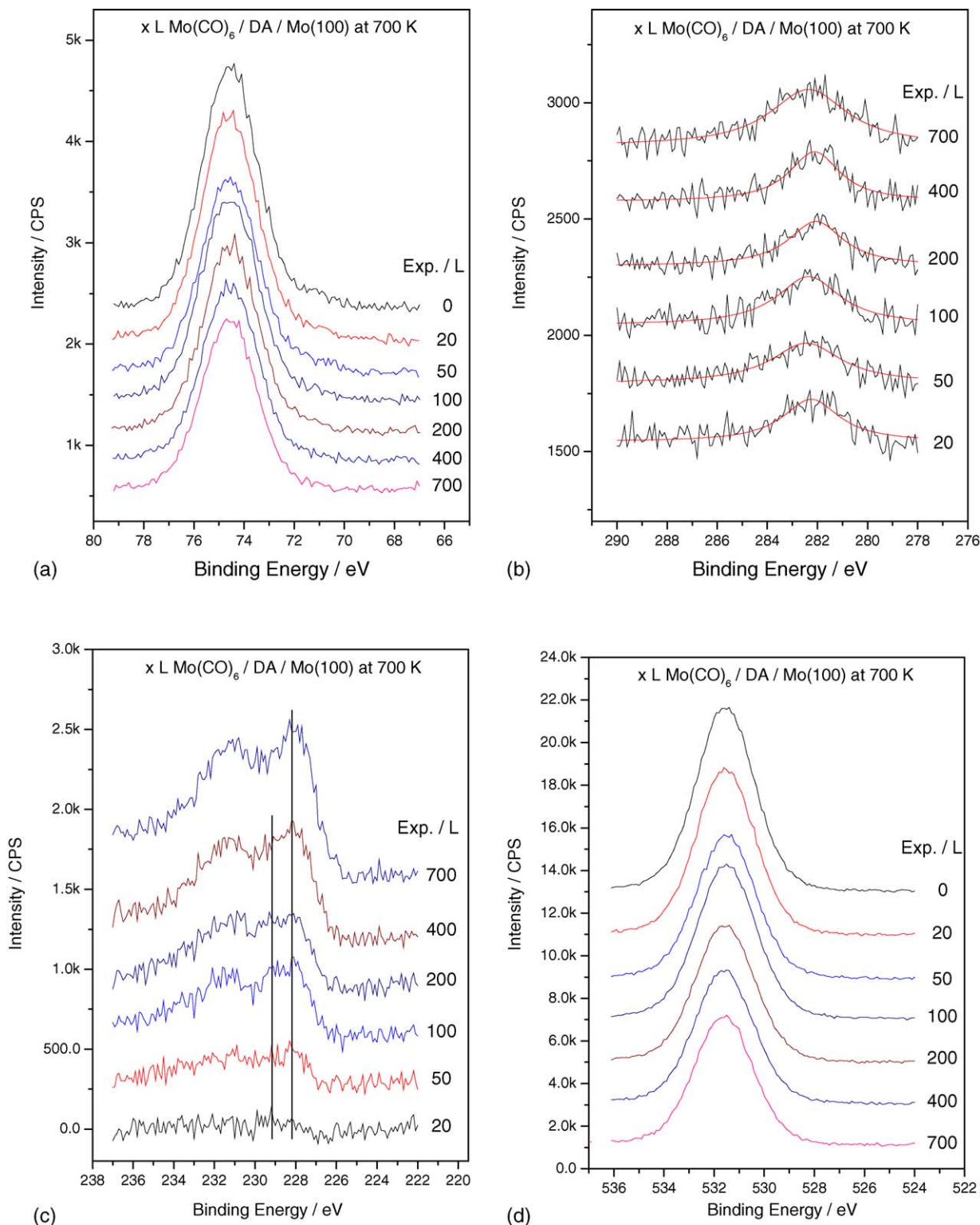


Fig. 4. Narrow scan Mg K $\alpha$  X-ray photoelectron spectra of the (a) Al 2p, (b) C 1s, (c) Mo 3d and (d) O 1s regions as a function of Mo(CO)<sub>6</sub> exposure on dehydroxylated alumina at 700 K, where exposures are displayed adjacent to the corresponding spectrum.

Spectrum 2) causes this feature to disappear suggesting that metallic aluminum is oxidized by Mo(CO)<sub>6</sub> at 700 K. Identical behavior is found for subsequent cycles. It should be mentioned that, following each TPD ex-

periment, the ratio Al<sub>65.7eV</sub>/Mo<sub>186eV</sub> remains relatively constant.

In order to identify the origin of the desorbing CO (Fig. 7(a)), an alumina film was grown using water contain-

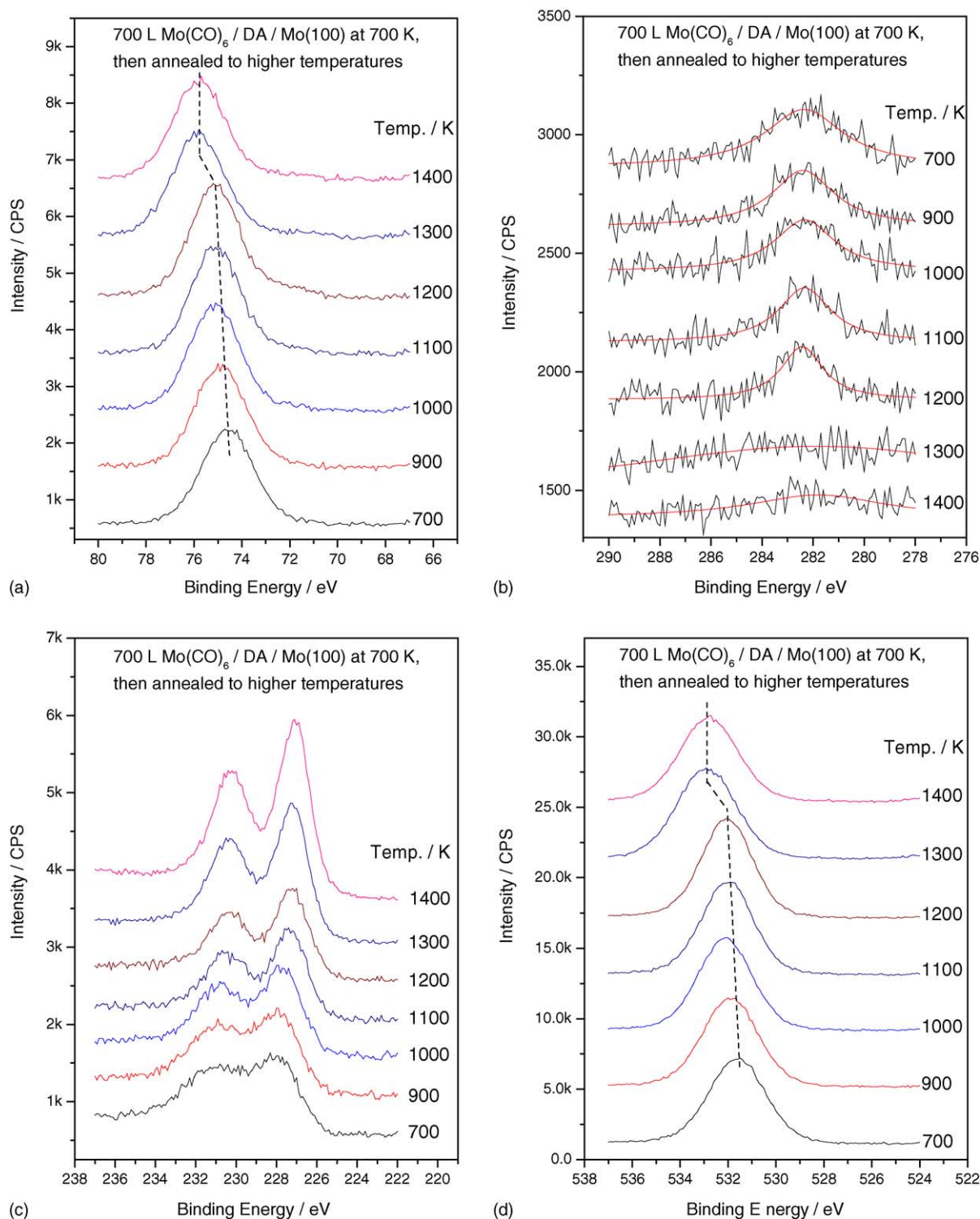
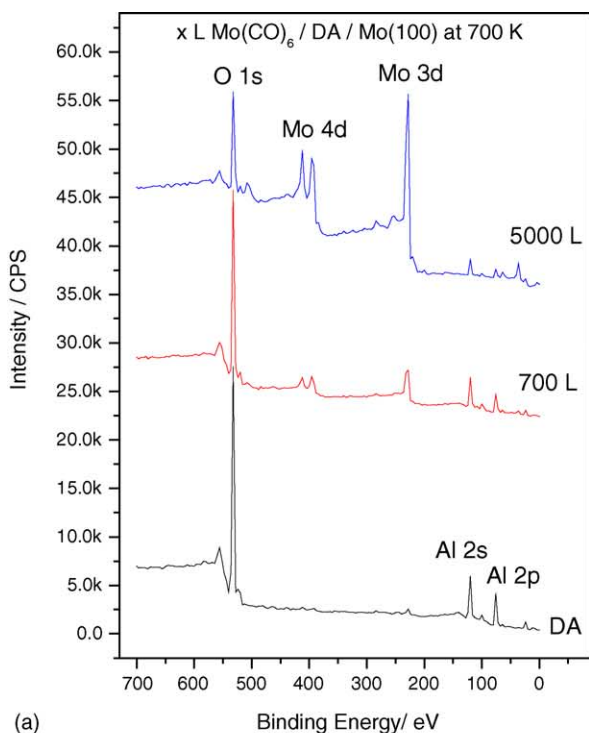


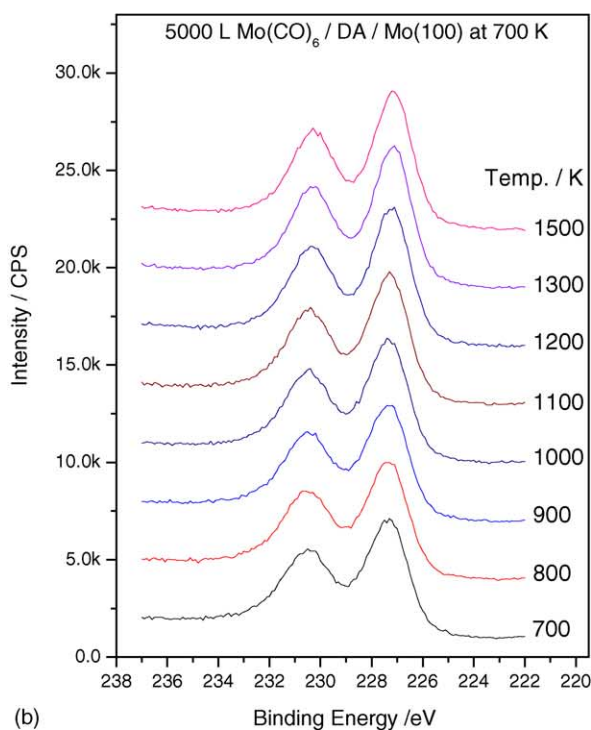
Fig. 5. Narrow scan Mg K $\alpha$  X-ray photoelectron spectra of the (a) Al 2p, (b) C 1s, (c) Mo 3d and (d) O 1s of 700 L of Mo(CO)<sub>6</sub> deposited onto dehydroxylated alumina at 700 K and heated to various temperatures, where annealing temperatures are displayed adjacent to the corresponding spectrum.

ing 10% H<sub>2</sub><sup>18</sup>O. Note that the carbonyl comprises C<sup>16</sup>O so that incorporation of <sup>18</sup>O into the CO that desorbs following molybdenum carbonyl reaction will indicate that the oxygen derives from the alumina. This surface was then reacted with 75 L of Mo(CO)<sub>6</sub> at various temperatures and the re-

sulting TPD spectra are displayed in Fig. 8. In this case, the 28 amu traces (C<sup>16</sup>O) have been attenuated by a factor of 10 compared to those collected at 30 amu (C<sup>18</sup>O). Since the water originally contained 10% H<sub>2</sub><sup>18</sup>O, equal intensity traces will indicate that the oxygen in the desorbing CO originates



(a)



(b)

Fig. 6. (a) Wide scan Mg  $K\alpha$  X-ray photoelectron spectra of DA, and with 700 and 5000 L  $\text{Mo}(\text{CO})_6$  adsorbed on dehydroxylated alumina at 700 K and (b) narrow scan Mg  $K\alpha$  X-ray photoelectron spectra of Mo 3d region following 5000 L  $\text{Mo}(\text{CO})_6$  exposure to DA at 700 K as a function of annealing temperature, where annealing temperatures are displayed adjacent to the corresponding spectrum.

exclusively from the alumina substrate. Dosing  $\text{Mo}(\text{CO})_6$  on dehydroxylated alumina at 500 K yields a small 28 amu desorption state at  $\sim 560$  K, which is absent in the 30 amu spectrum and this feature is assigned to subcarbonyl decomposition [13,15,16]. Two CO desorption states are found at higher temperatures comprising a broad feature between 800 and 1200 K and a sharper desorption state at  $\sim 1320$  K. For  $\text{Mo}(\text{CO})_6$  adsorption at 500 K, the low-temperature state is more intense at 28 amu than 30 amu, while the relative intensity of the 1320 K features at 28 and 30 amu correspond to the isotope ratio in the water that was used to grow the film. In the case of films grown from  $\text{Mo}(\text{CO})_6$  at 600 and 700 K, the broad feature between 800 and 1200 K is still more intense at 28 amu than 30 amu, but not as pronounced as the 500 K case.

## 4. Discussion

### 4.1. Nature of the deposited films

Molybdenum carbonyl decomposes on dehydroxylated alumina with a rather constant sticking probability where the rate of molybdenum uptake increases with increasing temperature (Fig. 2(a)). Both the carbon KLL Auger lineshape (Fig. 1(a)) and the C 1s binding energy (Fig. 4(b)) indicate that the carbon co-deposited with the molybdenum on dehydroxylated alumina at 700 K is carbidic in nature and the data of Fig. 2(b) indicates that the form of the carbide varies from MoC at low  $\text{Mo}(\text{CO})_6$  exposures, but becomes closer to  $\text{Mo}_2\text{C}$  as the exposure increases. Slight molybdenum oxidation is evidenced by the small changes in the intensity ratios of the molybdenum Auger peaks (Fig. 3). Mo has four strong features at 119, 160, 186 and 221 eV (Fig. 1(b)) due to  $M_{4,5}N_1N_{2,3}$ ,  $M_{4,5}N_1V$ ,  $M_{4,5}N_{2,3}V$  and  $M_{4,5}VV$  transitions, respectively [27]. It is expected that, during Mo oxidation, the  $M_{4,5}N_1N_{2,3}$  transition is the least perturbed since it involves core levels, while the  $M_{4,5}VV$  transition is the most sensitive since it involves both core levels and valence bands. The Mo  $3d_{5/2}$  binding energy shown in Fig. 4(c) may also indicate molybdenum oxidation, and will be discussed in more detail below.

The only changes observed in the Al 2p (Fig. 4(a)) and O 1s (Fig. 4(d)) XPS signals during  $\text{Mo}(\text{CO})_6$  dosing are a slight decrease in intensity due to attenuation of electrons by the molybdenum (oxy)carbide film. No changes in binding energy are observed following carbonyl adsorption at 700 K indicating that the alumina is not reduced at this temperature, in accord with the Auger data of Fig. 1(a). Because of the strong oxygen signals from the alumina substrate, the amount of oxygen adsorbed on the surface during  $\text{Mo}(\text{CO})_6$  deposition cannot be gauged using AES and XPS. However, the data plotted in Fig. 1(b) suggest that molybdenum is only slightly oxidized since no kinetic energy shift is observed for deposited molybdenum compared to the cleaned  $\text{Mo}(100)$  substrate. It has been demonstrated that heating

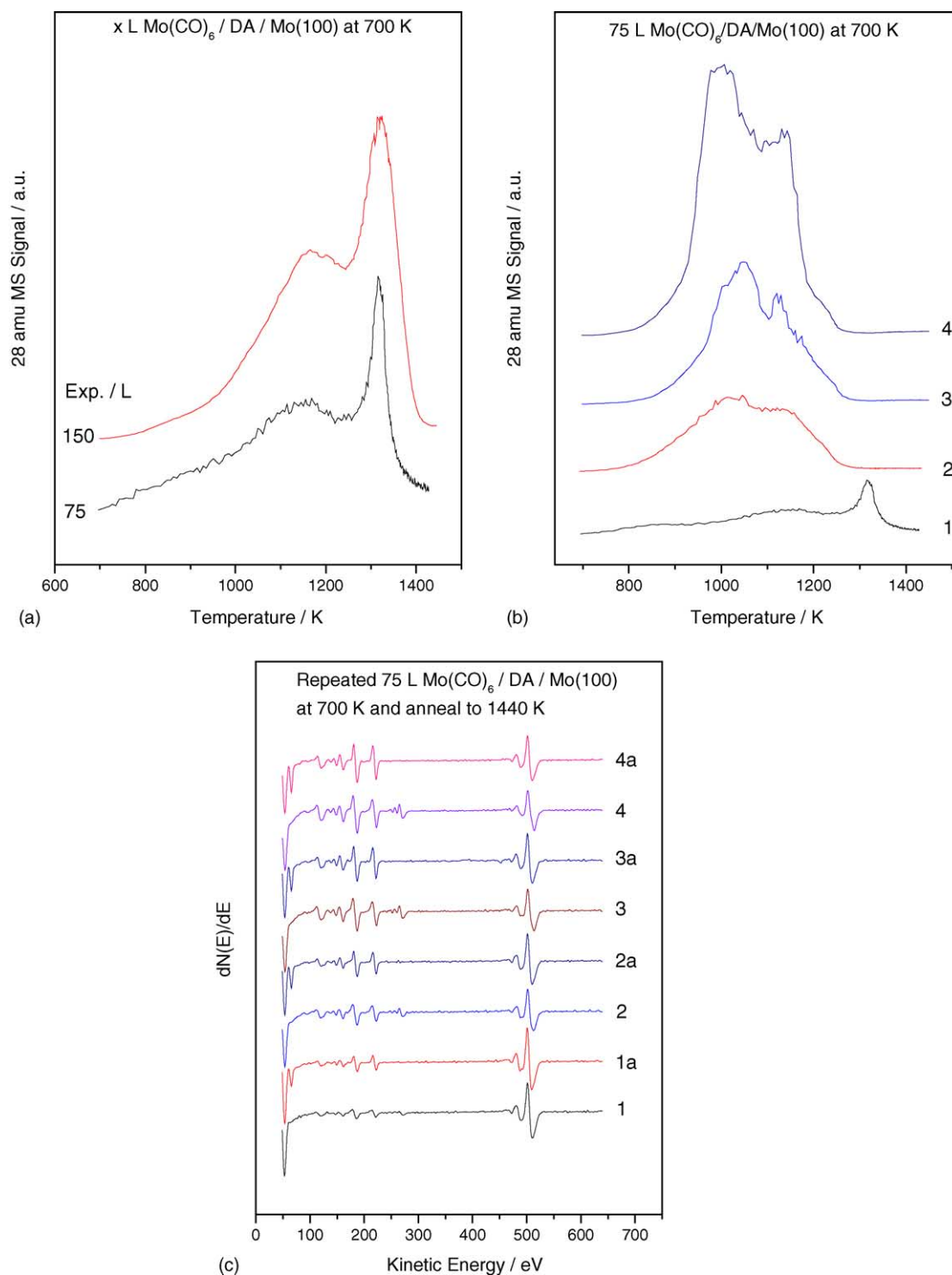


Fig. 7. (a) 28 amu (CO) temperature-programmed desorption spectra collected at a heating rate of 15 K/s for  $\text{Mo}(\text{CO})_6$  exposures of 75 and 150 L, (b) after repeated exposures of 75 L of  $\text{Mo}(\text{CO})_6$  after the previous TPD spectrum, (c) Auger spectra 1, 2, 3 and 4 after repeated exposure to 75 L of  $\text{Mo}(\text{CO})_6$  at 700 K and 1a, 1b, 1c and 1d, after the surface has been annealed to 1400 K.

$\text{Mo}(\text{CO})_x/\text{Si}(1\ 0\ 0)$  to 670 K leads to a film stoichiometry of  $\text{MoCO}_{0.3}$  [31], so that it is expected that the O/C ratio of the deposited film is substantially smaller than in that case.

It has been well established that complete decarbonylation of  $\text{Mo}(\text{CO})_6$  adsorbed on alumina occurs below 600 K

[13,15,16,32], and the carbide formation here is therefore due to CO disproportionation [33] as shown in Eqs. (1–3).



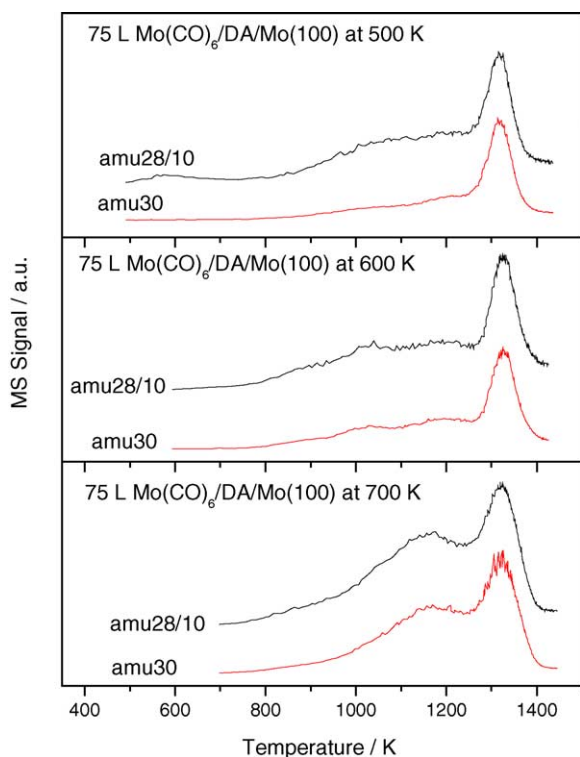
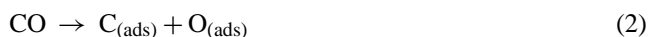


Fig. 8. 28 and 30 amu temperature-programmed desorption spectra collected at a heating rate of 15 K/s for 75 L  $\text{Mo}(\text{CO})_6$  adsorbed on dehydroxylated alumina formed using  $\text{H}_2\text{O}$  containing 10% of  $^{18}\text{O}$  at 500, 600 and 700 K, where the adsorption temperatures are indicated in the figure.



Evidently, if reaction (3) occurred exclusively, the surface carbide would be oxygen free. Clearly it is not the case. Stacy and co-workers [34,35] have demonstrated that oxygen is mobile in  $\text{Mo}_2\text{C}$  at room temperature and above. It is expected that if oxygen diffuses into the bulk, reaction (3) cannot occur so that CO dissociation on molybdenum carbide provides an alternative route for oxygen incorporation into the deposited film [36].

The Mo  $3d_{5/2}$  features at 228.1 and 229 eV BE (Fig. 4(c)) suggest molybdenum oxidation in accord with the Auger peak-to-peak intensity ratios (Fig. 3). However, there may be several origins of binding energy changes. First, carbide formation will result in an increase in binding energy, although this is small (typically smaller than 0.2 eV [37,38]). Second, while the Mo  $3d_{5/2}$  binding energy is relatively insensitive to low oxidation states ([39,40], and references therein), it is sensitive to changes in particle size for small particles, where it is found that core-electron binding energies increase monotonically with decreasing particle sizes [41–44]. Wertheim et al. [43,44] rationalized this behavior using a cluster-charge model, and proposed that the shift in binding energy of a free spherical cluster of radius  $r$ , is proportional to  $e^2/2r$ , independent of material. Since supported clusters are screened

by an image charge in the substrate, the binding energy shift is reduced to about half of the free-cluster value [44], and it has been found that that this model tends to underestimate the chemical shift for very small particles and overestimate it for large ones [42].

The data in Fig. 4(c) show that the deposited molybdenum carbide particles have Mo  $3d_{5/2}$  binding energies 0.7–1.6 eV larger than that of clean Mo(100). Assuming this is caused mainly by particle-size effects, particle sizes of  $\sim 1$ –3 nm are estimated from the free-cluster model. The intensity of the  $3d_{5/2}$  feature at 228.1 eV increases more rapidly than that at 229 eV with increasing  $\text{Mo}(\text{CO})_6$  exposure (Fig. 4(c)) indicative of particle growth. However, when 5000 L  $\text{Mo}(\text{CO})_6$  is deposited on dehydrogenated alumina at 700 K (Fig. 6(b)), a Mo  $3d_{5/2}$  binding energy of 227.4 eV is found. Note that this binding energy is identical to clean Mo(100) suggesting the formation of large particles or a thin molybdenum film so that the  $e^2/2r$  term contributes little to the chemical shift.

#### 4.2. Effect of annealing

Heating the molybdenum (oxy)carbide-covered, dehydroxylated alumina film to 1440 K causes substantial changes. Temperature-programmed desorption reveals that CO desorbs in two states at  $\sim 1130$  and 1320 K, and preparing the alumina with  $^{18}\text{O}$ -labeled water shows that both of these states include oxygen from the alumina substrate indicating that alumina is reduced by the carbide, as seen previously [14,21]. Alumina reduction is confirmed by the shift in Al 2p (Fig. 5(a)) and O 1s features (Fig. 5(d)) as a function of annealing temperature. There is a slight shift in oxidation state on annealing from  $\sim 900$  to  $\sim 1200$  K, associated with the lower-temperature CO desorption state and a large shift in the Al 2p state to 75.8 eV, and in the O 1s state to 533.2 eV binding energy when the surface is heated to 1300 K and above, coincident with the sharp  $\sim 1320$  K CO desorption feature. An aluminum Auger feature at 65.7 eV kinetic energy (Fig. 1(c)) implies the formation of some metallic aluminum. However, a shift in the Al 2p binding energy to 72 eV would be expected for metallic aluminum, but rather the binding energy increases to 75.8 eV (Fig. 5(a)). It is generally accepted that a binding energy increase of 2.5–2.8 eV from that of metallic Al 2p is a strong indication of the formation of stoichiometric alumina [45] (a shift of 2.6 eV is found here). The larger chemical shift ( $\sim 3.4$  eV) found here after  $\text{Mo}(\text{CO})_6$  adsorption and heating has been observed previously [46–49] and has been ascribed either to film thickness effects [47,48], or alumina reduction [46,49]. The larger shift is assigned, in this case, to alumina reduction since both the Auger data (Fig. 1(c)) and TPD results (Fig. 8) strongly support this conclusion. This larger shift is due to electron transfer from the reductively formed aluminum to the substrate, or at the adsorbate-substrate interface, leading to a contribution to the electrostatic potential resulting in a positive binding energy shift [49]. The O 1s feature shifts to higher binding energies as shown in Fig. 5(d) due to the same effect. Metallic

aluminum, on the other hand, since it donates electrons and is finely dispersed in an insulator (alumina), displays a binding energy increase [32].

Both the C 1s XP (Fig. 5(b)) and KLL Auger (Fig. 1(c)) spectra indicate that the surface is almost depleted of carbon on heating to  $\sim 1400$  K (after all the CO has desorbed (Figs. 7(a) and 8)). The molybdenum 3d<sub>5/2</sub> XPS signal shifts from 228.1 eV at 700 K to 226.9 eV at 1200 K, but then shows no further shift at higher temperatures (Fig. 5(c)). This binding energy is  $\sim 0.3$  eV below that of metallic molybdenum and this will be discussed further below. Furthermore, Fig. 3(d) indicates that molybdenum oxidation state decreases as the sample is heated to  $\sim 1200$  K. This suggests that the broad CO desorption state between 800 and 1200 K (Fig. 7(a)) is due partly to molybdenum oxycarbide decomposing to form a pure carbide. Note that the carbon Auger signal on annealing to above 1300 K is still carbidic (Fig. 1(a)). On the other hand, the data shown in Fig. 8 suggest that alumina reduction has started by 800 K as indicated by the observation of C<sup>18</sup>O desorption at this temperature. However, metallic aluminum is not detected until the sample is heated to above 1200 K (Fig. 1(c)). Presumably between 800 and 1200 K, the alumina is only partially reduced. In summary, the 1320 K CO desorption state is due to alumina reduction, while the state between 800 and 1200 K is due to the decomposition of the oxycarbide as well as partial reduction of alumina. This conclusion is supported by the data shown in Fig. 8 where it is apparent that the desorption intensity between 800 and 1200 K CO is larger at 28 than at 30 amu, while the intensity ratio of the 1300 K state corresponds to the initial isotope distribution. It is evident, from the data shown in Fig. 1(c) that, at 1000 and 1200 K, the C/Mo peak-to-peak intensity ratios are slightly higher than that at 700 K after a 750 L Mo(CO)<sub>6</sub> exposure (Fig. 1(a)). This is due to carbon diffusion to the near-surface region during annealing and has been demonstrated previously for  $\alpha$ -Mo<sub>2</sub>C [50].

As discussed previously, the incorporation of C and O does not cause a Mo 3d binding energy shift and this is mainly ascribed to a particle-size effect. Correspondingly, therefore, CO desorption cannot be the reason for the Mo 3d binding energy decrease found in Fig. 5(c), although it is clear that molybdenum is reduced during annealing as indicated by the Auger peak-to-peak intensity ratios (Fig. 3(d)). There are two possible origins for this phenomenon. First, it might be due to particle agglomeration where the  $e^2/2r$  term contributes less to the chemical shift when particle sizes become larger. This is not very likely since no decrease is found in the Mo 3d<sub>5/2</sub> signal intensity. Alternatively, it could be due to alumina reduction so that the substrate is no longer a perfect insulator. In this case, the core hole can be rapidly neutralized so that the electrostatic particle-size contribution is diminished [44]. This notion is corroborated by the fact that, when Mo(CO)<sub>6</sub> is deposited onto metallic aluminum at 700 K, no particle-size-induced Mo 3d chemical shift is observed [21].

The above discussion indicates that the 1320 K CO desorption feature is due to a high-temperature reduction of the

alumina by molybdenum carbide. The resulting surface contains little carbon (Figs. 1(c) and 5(b)) but exhibits a Mo 3d<sub>5/2</sub> binding energy that is 0.3 eV below that of metallic molybdenum. A similar effect has been observed previously for Mo(CO)<sub>6</sub> adsorbed on metallic aluminum at 700 K and annealed to 1200 K, where both the Mo and Al binding energies decreased [21], and was assigned to the formation of a MoAl alloy. Al-transition-metal alloys (aluminides) have been studied extensively, where the aluminum core levels generally shift to binding energies lower than those of metallic aluminum, and the binding energies of the transition metals also normally shift to lower binding energies, with the exception of Ni and Pd [48,51–54]. Theoretical calculations [54] suggest that the electron density within both aluminum and the transition metal increases at the expense of the interstitial regions. The Mo 3d binding energy decrease here is therefore similarly assigned to MoAl alloy formation. Note that metallic aluminum is detected by AES (Figs. 1(c) and 7(c)) but not by XPS (Fig. 5(a)). This suggests that aluminum is highly dispersed on the surface so that no large aluminum domains are formed [32], otherwise a 72 eV feature would be detected. The Mo 3d signal intensity increase at 1300 K (Fig. 5(c)) is presumably due to Mo spreading on the surface and similar behavior has been seen previously with a Ni/Al<sub>2</sub>O<sub>3</sub> [55].

Finally, the effect of repeated Mo(CO)<sub>6</sub> exposure and annealing is addressed (Fig. 7(b)). Note that the CO desorption behavior changes drastically after the first exposure. In subsequent cycles, more CO desorbs from the surface while the  $\sim 1320$  K state disappears. Following initial adsorption and annealing, metallic molybdenum (in the form of a MoAl alloy) is deposited on the surface and will adsorb CO during subsequent Mo(CO)<sub>6</sub> exposures. High-temperature CO desorption has been found previously from Mo(1 0 0) at 840, 940 and 1250 K [56] and at  $\sim 1000$  K on Mo(1 1 0) [57]. A CO desorption temperature of  $\sim 990$  K was also found following formic acid decomposition on Mo(1 1 0) [58] in accord with the temperatures observed in temperature-programmed desorption (Fig. 7(b)), consistent with these states being due to C + O recombination. Following each Mo(CO)<sub>6</sub> adsorption and desorption cycle, more metallic aluminum is formed (Fig. 7(c)), and the TPD profiles shown in Fig. 7(b) also contain CO from alumina reduction during subsequent cycles. It is not apparent why the 1320 K CO desorption state disappears after the first cycle. Presumably this is related to MoAl alloy formation.

## 5. Conclusions

The reaction of molybdenum hexacarbonyl with a thin dehydroxylated alumina film grown on a Mo(1 0 0) substrate at temperatures between 500 and 700 K results in the formation of molybdenum carbide that incorporates a small amount of oxygen. The Mo:C stoichiometry varies with Mo(CO)<sub>6</sub> exposure so that the surface carbide is close to MoC for low exposures, tending to Mo<sub>2</sub>C when the carbonyl exposure in-

creases. Heating the surface results in two CO desorption states at  $\sim 1130$  and  $1320$  K, where isotope labeling the alumina indicates that the oxygen derives largely from the substrate. The low-temperature CO desorption state appears to arise from molybdenum oxycarbide decomposition and alumina reduction, while the high-temperature state is due to alumina reduction by molybdenum carbide. This results in the formation of an alloy between the aluminum and molybdenum.

## Acknowledgment

We gratefully acknowledge support of this work by the Chemistry Division of the National Science Foundation under grant number CTS-0105329.

## References

- [1] A. Brenner, *J. Mol. Catal.* 5 (1979) 157.
- [2] E. Davie, D.A. Whan, C. Kemball, *J. Catal.* 24 (1972) 272.
- [3] J. Smith, R.F. Howe, D.A. Whan, *J. Catal.* 34 (1974) 191.
- [4] R. Thomas, J.A. Moulijn, *J. Mol. Catal.* 15 (1982) 157.
- [5] A. Brenner, R.L. Burwell Jr., *J. Am. Chem. Soc.* 97 (1975) 2565.
- [6] A. Brenner, R.L. Burwell Jr., *J. Catal.* 52 (1978) 353.
- [7] R.F. Howe, *Inorg. Chem.* 15 (1976) 486.
- [8] A. Kazusaka, R.F. Howe, *J. Mol. Catal.* 9 (1980) 183.
- [9] K.P. Reddy, T.L. Brown, *J. Am. Chem. Soc.* 117 (1995) 2845.
- [10] A. Zecchina, E.E. Platero, C.O. Areán, *Inorg. Chem.* 27 (1988) 102.
- [11] R.F. Howe, I.R. Leith, *J. Chem. Soc., Faraday Trans. I* 69 (1973) 1967.
- [12] W.M. Shirley, B.R. McGarvey, B. Maiti, A. Brenner, A. Cichowlas, *J. Mol. Catal.* 29 (1985) 259.
- [13] M. Kaltchev, W.T. Tysoe, *J. Catal.* 193 (2000) 29.
- [14] M. Kaltchev, W.T. Tysoe, *J. Catal.* 196 (2000) 40.
- [15] Y. Wang, F. Gao, M. Kaltchev, D. Stacchiola, W.T. Tysoe, *Catal. Lett.* 91 (2003) 88.
- [16] Y. Wang, F. Gao, M. Kaltchev, W.T. Tysoe, *J. Mol. Catal. A: Chem.* 209 (2004) 135.
- [17] Z. Jiang, W. Huang, J. Jiao, H. Zhao, D. Tan, R. Zhai, X. Bao, *Appl. Surf. Sci.* 229 (2004) 43.
- [18] C.C. Williams, J.G. Ekerdt, *J. Phys. Chem.* 97 (1993) 6843.
- [19] L. Rodrigo, K. Marcinkowska, P.C. Roberge, S. Kaliaguine, *J. Catal.* 107 (1987) 8.
- [20] I.V. Elav, B.N. Shelimov, V.B. Kazansky, *J. Catal.* 113 (1988) 256.
- [21] Y. Wang, F. Gao, W.T. Tysoe, *J. Mol. Catal. A: Chem.* 236 (2005) 18.
- [22] M.G. Kaltchev, A. Thompson, W.T. Tysoe, *Surf. Sci.* 391 (1997) 145.
- [23] W.J. Wytenburg, R.M. Lambert, *J. Vac. Sci. Technol. A* 10 (1992) 3597.
- [24] P.J. Chen, M.L. Colaianni, J.T. Yates Jr., *Phys. Rev. B* 41 (1990) 8025.
- [25] D. Briggs, M.P. Seah, *Practical Surface Analysis: Auger and X-ray Photoelectron Spectroscopy*, John Wiley & Son, 2004.
- [26] D. Briggs, J.T. Grant (Eds.), *Surface Analysis by Auger and X-ray Photoelectron Spectroscopy*, IM Publications and Surface Spectra Limited, UK, 2003.
- [27] C. Zhang, M.A. Van Hove, G.A. Somorjai, *Surf. Sci.* 149 (1985) 326.
- [28] A. Wolowik, M. Janik-Czachor, *Mater. Sci. Eng. A* 267 (1999) 301.
- [29] B.R. Strohmeier, *Surf. Sci. Spectra* 3 (1995) 135.
- [30] K. Edamoto, M. Sugihara, K. Ozawa, S. Otani, *Surf. Sci.* 561 (2004) 101.
- [31] J.R. Creighton, *J. Appl. Phys.* 59 (1986) 410.
- [32] M. Kurhinen, S. Myllyoja, M. Suvanto, T.A. Pakkanen, *J. Mol. Catal. A: Chem.* 154 (2000) 229.
- [33] G. Henrici-Olive, S. Olive, *The Chemistry of the Catalyzed Hydrogenation of Carbon Monoxide*, Springer-Verlag, Berlin Heidelberg, 1984.
- [34] K.J. Leary, J.N. Michaels, A.M. Stacy, *J. Catal.* 101 (1986) 301.
- [35] K.J. Leary, J.N. Michaels, A.M. Stacy, *J. Catal.* 107 (1987) 393.
- [36] L. Bugyi, F. Solymosi, *J. Phys. Chem. B* 105 (2001) 4337.
- [37] J.A. Rodriguez, J. Dvorak, T. Jirsak, *J. Phys. Chem. B* 104 (2000) 11515.
- [38] J.M. Horn, Z. Song, D.V. Potapenko, J. Hrbek, M.C. White, *J. Phys. Chem. B* 109 (2005) 44.
- [39] T. Schoreder, J. Zegenhagen, N. Magg, B. Immaraporn, H.-J. Freund, *Surf. Sci.* 552 (2004) 85.
- [40] H.H. Hwu, J.G. Chen, *Chem. Rev.* 105 (2005) 185.
- [41] P. Legare, Y. Sakisaka, C.F. Brucker, T.N. Rhodin, *Surf. Sci.* 139 (1984) 316.
- [42] V. Murgai, S. Raaen, M. Strongin, R.F. Garrett, *Phys. Rev. B* 33 (1986) 4345.
- [43] G.K. Wertheim, S.B. DiCenzo, S.E. Youngquist, *Phys. Rev. Lett.* 51 (1983) 2310.
- [44] G.K. Wertheim, S.B. DiCenzo, *Phys. Rev. B* 37 (1988) 844.
- [45] D.L. Cocke, E.D. Johnson, R.P. Merrill, *Catal. Rev.-Sci. Eng.* 26 (1984) 163.
- [46] M. Gautier, J.P. Duraud, L. Pham Van, M.J. Guittet, *Surf. Sci.* 250 (1991) 71.
- [47] A. Jimenez-Gonzalez, D. Schmeisser, *Surf. Sci.* 250 (1991) 59.
- [48] Y. Wu, H.-S. Tao, E. Garfunkel, T.E. Madey, N.D. Shinn, *Surf. Sci.* 336 (1995) 123.
- [49] J. Libuda, M. Frank, A. Sandell, S. Andersson, P.A. Bruhwiler, M. Baumer, N. Martensson, H.-J. Freund, *Surf. Sci.* 384 (1997) 106.
- [50] T.P. St. Clair, S.T. Oyama, D.F. Cox, S. Otani, Y. Ishizawa, R.-L. Lo, K. Fukui, Y. Iwasawa, *Surf. Sci.* 426 (1999) 187.
- [51] N.R. Gleason, D.R. Strongin, *Surf. Sci.* 295 (1993) 306.
- [52] V. Shutthanandan, A.A. Saleh, R.J. Smith, *Surf. Sci.* 450 (2000) 204.
- [53] N.R. Shivaparan, V. Shutthanandan, V. Krasemann, R.J. Smith, *Surf. Sci.* 373 (1997) 221.
- [54] P.A. Schultz, J.W. Davenport, *Scripta Metall.* 27 (1992) 629.
- [55] J.G. Chen, J.E. Crowell, J.T. Yates Jr., *Surf. Sci.* 185 (1987) 373.
- [56] F. Zaera, E. Kollin, J.L. Gland, *Chem. Phys. Lett.* 121 (1985) 464.
- [57] M.L. Colaianni, J.G. Chen, W.H. Weinberg, J.T. Yates Jr., *J. Am. Chem. Soc.* 114 (1992) 3735.
- [58] C. Xu, D.W. Goodman, *J. Phys. Chem.* 100 (1996) 1753.